American Mineralogist, Volume 83, pages 1141–1151, 1998

Magmatic sulfur compounds and sulfur diffusion in albite melt at 1 GPa and 1300–1500 °C

K. Tobias Winther,[1,*] E. Bruce Watson,[1] and Gerald M. Korenowski[2]

[1]Department of Earth and Environmental Sciences, Rensselaer Polytechnic Institute, West Hall G17, 110 8th Street, Troy, New York 12180–3590, U.S.A.

[2]Department of Chemistry, Rensselaer Polytechnic Institute, 110 8th Street, Troy, New York 12180–3590, U.S.A.

Abstract

The speciation and diffusion of sulfur in nominally dry albite melt at 1300–1500 °C has been investigated by analyzing glasses formed in piston-cylinder runs using electron microprobe, micro-Raman, infrared-, UV-, and visible-light-spectroscopy, and other techniques. The sulfate ion is very stable in the albite melt even at low f_{O_2} and is the dominant species in all glasses. In the presence of graphite the glass acquired a characteristic strong violet color, as a consequence of conversion of some of the sulfate to S_2^- and S_3^- radical anions. The equilibration between S_2^- and S_3^- was rapid and both radicals were found to be very stable at elevated temperatures. Both S_2^-, S_3^-, and sulfide diffuse faster then the sulfate anion, so these species will control the diffusion process when present. In violet-colored albite glass in which some of the sulfur is S_2^- and S_3^-, the diffusion coefficient for bulk sulfur diffusion was found to be:

$$D = 14.7 \exp\left(\frac{-458100\ J \cdot mol^{-1}}{RT}\right)\frac{m^2}{s}$$

where T is the temperature in K and R the gas constant. This relation defines D values significantly lower than those determined for sulfur in dry andesite, dacite, and rhyolite melt, in which the diffusion is controlled by sulfide. The reason for this difference is the higher degree of melt polymerization, the stabilization of sulfate over sulfide in the albite melt, and the slow diffusion of S_2^- and S_3^- radical anions compared to sulfide.

Introduction

Sulfur is present in small but significant quantities in magmas of a wide variety of compositions (e.g., Carroll and Rutherford 1988). During magma ascent and crystallization, sulfur can be ''partitioned'' in several ways: sulfur-bearing minerals such as pyrrhotite and anhydrite may crystallize; an immiscible sulfur melt may form; sulfur may be incorporated as a trace element in many minerals (Ricke 1960); and it may enter the volatile phase, which can be either trapped in fluid inclusions or ultimately released to the environment (Kress 1997).

The diffusion of sulfur in magmas is important in controlling formation of bubbles and sulfur-bearing phases. However, the different dissolved species have different rates of diffusion and knowing the speciation therefore becomes critical. Additionally, the different species have different solubilities in the magmas, which determine the onset and growth of different magmatic sulfur minerals and bubbles; the different species also have different partitioning between melt and crystalline/vapor phases, and they have different roles in the overall melt structure and thus influence the physical properties of the melt in different ways.

Sulfur exists in six different oxidation states; however, only four of them, namely −2, −1, 0, and +6, are commonly found in natural environments on earth and only two (−2 and +6) are common in silicate melts (Baker and Rutherford 1996). Many sulfur-bearing species have been reported from natural systems including: SO_4^{2-}, S^{6+}, S^{2-}, COS, CS_2, SO_2, SO_3, S_2^-, S_3^-, H_2S, S, H_2SO_4 (e.g., Baker and Rutherford 1996; Cotton et al. 1976; Fincham and Richardson 1954; Gerlach and Nordlie 1975a and 1975c). The S^{2-} anion can substitute for O^{2-} in the silicate network whereas S^{6+} can form SO_4^{2-}. Many studies have addressed the speciation and solubility of sulfur in magmatic systems (e.g., Bradbury 1983; Carroll and Rutherford 1988; Gerlach and Nordlie 1975a, 1975c; Haughton et al. 1974; Mathez 1976; Mysen and Dick 1977; Mysen and Popp 1980; Poulson and Ohmoto 1990). Only a few studies have addressed the diffusion of the various species in magmatic systems. The paper by Baker and Rutherford (1996) is based on dissolution of anhydrite and pyrrhotite into a rhyolite melt. Their experimental setup makes coupled diffusion involving calcium and sulfur or iron and sulfur unavoidable. In addi-

* E-mail: winther@cat.rpi.edu

0003–004X/98/1112–1141$05.00

TABLE 1. Microprobe analyses* of starting materials

Sample	Albite	Albite (with S)
SiO_2	68.2	68.4
Al_2O_3	19.3	19.6
Na_2O	11.1	11.3
ZrO_2	0.12	0.01
GeO_2	0.18	0.00
Ga_2O_3	0.14	0.00
FeO	0.00	0.01
S	0.00	0.11
Total	99.0	99.4

Note: The sulfur-bearing glass contain approximately 0.1% H_2O while the sulfur-free glass contain approximately 0.05%. The sodium values are slightly low due to volatilization of sodium during analysis.
* In weight percent.

tion, the presence of a multivalent element like iron raises questions as to its potential influence on the oxidation state of sulfur. Previous work by Watson et al. (1993) and Watson (1994) was of limited scope and restricted to diffusion of the sulfide ion.

The focus of this work is to study the diffusion of sulfur in a simple silicate melt. Albite was chosen as the melt composition because it contains few elements, none of which occur in different oxidation states in nature. The experiments were set up using a diffusion couple consisting of two glasses with identical compositions, except for a trace amount of sulfur in one of them. It became clear that all the sulfur-doped glass produced contained trace amounts of carbon impurities. There were several potential sources of carbon contamination: organic solvents used for grinding; fine dust from the air; and diffusion from the graphite furnace used in the experimental setup. Sulfur-free glasses were fired in air at high temperatures (up to ~1000 °C), and in general did not contain carbon; however, the sulfur-bearing glass could not be fired as this would cause a sulfur loss. As carbon is present in most natural systems the carbon contamination makes the experiments more relevant to geological problems, and we decided to characterize the system rather than attempting to eliminate the carbon contamination. In this way the two main objectives of this paper became: (1) characterize the S compounds present in albite with S-C-O-H, and (2) investigate sulfur diffusion in this system.

EXPERIMENTAL PROCEDURE

Starting materials

Synthetic albite was made from high purity SiO_2, Al_2O_3, and Na_2CO_3 (Table 1). In some cases, 1000–4000 ppm Si was replaced by equal stoichiometric amounts of Zr and Ge (introduced as ZrO_2 and GeO_2), whereas 1000–2000 ppm Al was replaced by equal stoichiometic amounts of Ga (added as Ga_2O_3). The Zr, Ge, and Ga diffusion profiles were used to mark the original interface in the diffusion couples. The starting material was melted two times in a platinum crucible in air at ~1300 °C for 15 min. The CO_2 was lost from the carbonate during this process. Before, between, and after melting the material, it was carefully homogenized by grinding in an agate mortar with high-purity ethanol.

Synthetic albite glass with dissolved sulfur was made by first producing an albite glass as described above, except for a minor sodium deficit. Then Na_2SO_4 was added to achieve the correct sodium level. This sample was melted two times at 1400 °C, 1 GPa for 1 h and homogenized before and between the melting by grinding in an agate mortar with high-purity ethanol. To ensure retention of sulfur in the sulfur-bearing samples, they were not fired at high temperature in air after the grinding in alcohol. This may have caused the presence of traces of residual carbon in the sample. In addition, lint from the air seems to have caused some minor carbon contamination. In some samples some of the Na_2O was replaced by $NaNO_3$, introducing a total of 1000–2000 ppm NO_2 to the sample. The nitrate helped oxidize the carbon to form CO_2 rather than graphite.

The diffusion couple was made by filling the lower part of the capsule with albite powder and placing a piece of polished, sulfur-doped glass above it. Ground, sulfur-doped glass was packed around the glass piece. If both sides of the diffusion couple contained sulfur, the material with the lower sulfur concentration was packed as a powder in the lower part of the capsule. Some experiments were done using other materials such as albite with graphite or barite to investigate the formation of radicals rather than obtaining only diffusion data. All starting materials were dried for at least 12 h at 105–110 °C prior to the experiment. In a few cases, sulfur-free starting materials were dried at 700 °C.

Experimental technique

High-pressure experiments were performed in a 0.75″ (19 mm) piston-cylinder apparatus. In diffusion experiments, the sample capsules were made from hard alumina lined on the outside with an oxidized iron sleeve (Fig. 1). This sleeve helped maintain the structural integrity of the sample after the experiment, and the Fe_2O_3 was intended to keep the environment oxidized. It was, however, not always the case that the iron oxide was preserved throughout the experiment. The capsules were placed inside crushable alumina parts fitting into a graphite furnace. In synthesis runs the powder was placed inside the crushable alumina, either with or without a hard alumina container. Outside the graphite furnace was a Pyrex glass sleeve, a salt cylinder, and a sheet of lead foil. The temperature was controlled using a W-Re thermocouple.

Analytical methods

The samples were analyzed using an electron microprobe (JEOL 733 Superprobe). An expanded electron beam (20 or 30 μm in diameter) was used with 15 kV acceleration voltage and a cup current of 12–75 nA. Currents up to 125 nA were used for measuring the sulfur peak position. For peak position measurements, an exact focusing of the beam on the surface is essential because

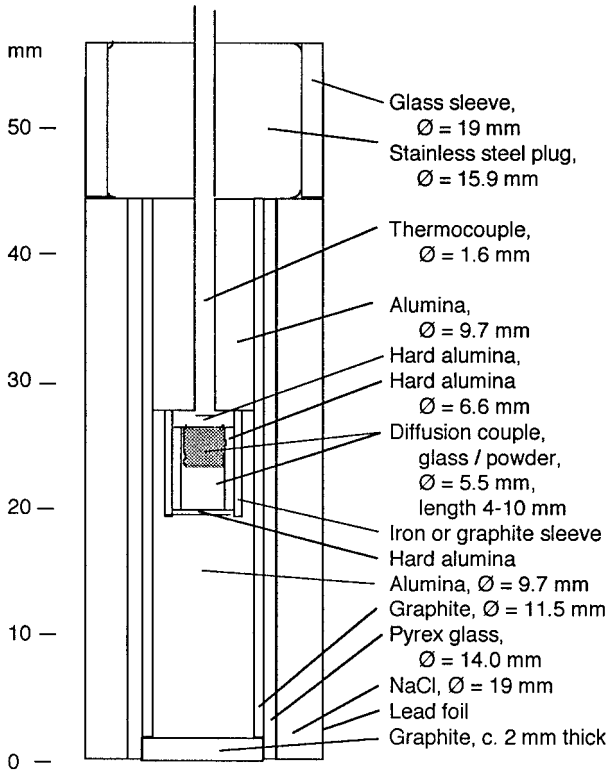

FIGURE 1. Diagram of the cell used in the experimental setup. The outer diameter, Ø, is shown in millimeters.

of its effect on the sample-detector geometry. If the sample is out of focus an apparent shift in the peak position by as much as 0.052 ° 2θ angle can occur (0.1 mm on the PET crystal spectrometer on the JEOL microprobe used). Potentially, pits burned in the surface of the sample could cause a change in the position of surface and thereby in the apparent peak position, and beam damage to the sample could cause changes in the sulfur speciation. However, repeated wavelength scans at the same position showed that the peak did not change position when the sample was damaged. What did change was the count rate of sulfur, which goes up with increased damage whereas the background count rate remains the same thereby giving results that are too high. This change in apparent sulfur concentration was found to be larger than what could be expected as a result of decreasing sodium content in the glass alone.

A Perkin-Elmer FTIR was used to obtain spectra of doubly polished glass disks. Micro Raman spectra were obtained using a T64000 Raman Spectrum system from JOBIN YVON-SPEX with a 514 nm laser. A few spectra were obtained using a Nicolet Raman 950 system with a 1064 nm laser. UV and visible-light spectra were obtained on a Hitachi U-2000 spectrophotometer running against air and scanning the wavelength range 150–1100 nm. An ESR (Electron Spin Resonance) spectrum was obtained from a Varian E9 ESR system using a time constant of 0.3 s, a modulation amplitude of 0.5 G, a microwave power of 0.02 W, and a scan time of 8 min.

The diffusion coefficients were determined by minimizing the difference between the observed data and an ideal diffusion profile calculated with the diffusion coefficient, the interface position, the high concentration, and the low concentration as variables to be optimized.

EXPERIMENTAL RESULTS: SULFUR COMPOUNDS

The conditions and results of selected runs are shown in Tables 2 and 3. Glasses of albite and sulfate-bearing albite are clear or slightly cloudy. If a graphite seed is planted in a sulfate-bearing glass and maintained at 1400 °C and 1 GPa for 1 h, a violet halo 40–90 μm in diameter develops around the seed, reflecting the diffusion of carbon and/or oxygen and reaction with the sulfate. The size of the halo suggests that it is controlled by a species diffusing more or less with the same speed as sulfur, which could be oxygen. Over time, a carbon-bearing glass, especially after re-homogenization, will develop a strong characteristic violet color throughout. If a diffusion couple is prepared with violet, sulfur-bearing glass placed against clear sulfur-free glass, the violet color will not fade to clarity until the very end of the diffusion profile (<100 ppm S), and the sulfur-bearing part remains violet even after runs of 50 h. As shown below, this color is attributed to the presence of S_2^- and S_3^- radical anions. Most of the glass samples used fall in one of the following categories: albite; albite with sulfate; albite with sul-

TABLE 2. Run conditions and results of selected diffusion experiments

Run id.	Temperature (°C)	Pressure (GPa)	Time (h)	High sulfur (ppm)	Low sulfur (ppm)	Sulfur D (10^{-14} m²/s)	Zirconium D (10^{-14} m²/s)
0124	1400	1.04	5	325	0	6.39	3.25
0126	1400	1.04	5	994	457	5.81, 5.92	2.38
0214	1400	1.04	50	433	0	5.03, 6.96	0.87, 1.65
0217	1400	1.05	50	1140	479	4.62, 6.72	1.09, 2.74
0221	1400	1.03	50	1107	0	4.62, 4.24	2.65, 3.30
0310	1300	1.05	68	1026	1	1.00	1.2
0314	1500	1.05	5	1126	44	52.9	
0702	1400	1.00–1.08	9.28	1239	0	11.2, 28.1	
0707	1400	1.10	4.00	1185	0	11.6, 19.0	
0718	1400	1.09	4.00	1366	10	64.9	
1030	1400	1.07–1.08	9.62	1398	0	22.5	

Note: Samples 0702, 0707, and 0718 contain sodium nitrate and were less strongly violet than the other samples.

TABLE 3. Run conditions of selected synthesis runs and runs for investigating the sulfur sepciation

Run id.	*T* (°C)	*P* (GPa)	Time (h)	Sulfur (ppm)	Comments
0107	1400	1.05	1.0	≈1500	clear except few violet spots
0219	1400	1.08	1.0	≈1500	violet glass
0307	1400	1.08	1.0	≈1500	violet glass
0313	1400	1.07	4.0	0/20 000	albite w/2% sulfate in graphite container
0315	1400	0.99	13.4	0	0.8% graphite, black
0316	1400	1.05	1.0	≈1500	homogenized in water (no ethanol)
0317	1400	1.05	1.0	≈1500	homogenized in water (no ethanol)
0408	1400	1.05	4.0		barite-albite no graphite
0409	1400	1.05	4.0		barite-albite w/675 ppm C as graphite
0410	1400	1.05	4.0		barite-albite w/8000 ppm C as graphite
0414	1400	1.05	1.0		albite with 675 ppm C as CO_2
0415	1400	1.05	2.0		albite above albite w/Ga, Ge, and Zr
0416	1400	1.05	2.0		barite-albite no graphite
0417	1400	1.05	2.0		barite-albite w/675 ppm C as CO_2
0418	1400	1.05	2.0		barite-albite w/675 ppm C as graphite
0421	1400	1.05	1.0		albite w/675 ppm CO_2, 1000 ppm excess O_2 from $NaNO_3$ and Zr, Ge, Ga
0422	1400	1.05	2.0		barite-albite w/CO_2 (0421)
0423	1400	1.05	2.0		barite-albite w/675 ppm graphite, no Pt
0424	1400	1.05	2.0		as 0423 but with Pt sleeve
0425	1400	1.05	2.0		barite-albite (decarbonated at 1093 °C)
0426	1400	1.05	1.0		re-melting of 0316 and 0317
0506	1400	1.05	16.8		barite/albite heated to >900 °C
0511	1400	1.06	1.0		albite w/675 ppm C as CO_2 plus NO_x
0613	1400	1.05	1.25		violet S-bearing albite glass in capsule w/Zr lid and Ti bottom. Color vanished near metal.
0618	1400	1.04	1.0		violet glass + Al_2O_3 + SiO_2 + $NaNO_3$
0626	1400	1.06	1.0		albite w/Na_2NO_3, $NaSO_4$, Al_2O_3, SiO_2
0627	1400	1.06	1.0		albite w/Na_2NO_3, $NaSO_4$, Al_2O_3, SiO_2
0628	1400	1.05	1.0		0626 + 0627
1018	1400	1.10	1.0	0	albite (no sulfur)
1213	1400	1.04	3.0		albite + Si + Al + Na_2SO_4

Note: 0408-10 were done in one experiment. 0415-18 were done in one experiment. 0422-25 were done in one experiment with the capsule slightly below the furnace center. The following experiments had graphite or carbon bearing compounds added on purpose: 0313, 0315, 0409, 0410, 0414, 0417, 0418, 0421, 0422, 0423, 0424, and 0511. In all other cases any carbon that may be present originated as "uncontrolled" contamination.

fate and graphite; albite with sulfate and nitrate; and albite with sulfate, carbon dioxide, and nitrate. The nitrate was introduced into some samples in an attempt to maintain oxidized conditions. The samples were investigated using many techniques as described below.

Infrared (FTIR) spectroscopy

All FTIR spectra collected show an OH absorption peak around 3510 cm^{-1}. The sulfur-bearing glasses show in addition a CO_2 peak at 2350 cm^{-1}. The 3510 cm^{-1} OH stretching absorption band was used to estimate the water content using the calibration of Silver and Stolper (1989). Sulfur-free glass (sample 1018) has 0.05 wt% water, whereas the sulfur-bearing glasses (samples 0107, 0219, and 0307) have 0.09–0.11 wt% water. The sulfur-bearing glasses are expected to have higher water contents because they were not fired in air at high temperature (which causes sulfur loss). Using the absorptivity coefficient of Fine and Stolper (1985), the concentrations of CO_2 were calculated: The sulfur-free glass (1018) has 0 ppm; the non-violet sulfur-bearing glass (0107) has 78 ppm; and the violet sulfur-bearing glass has 100 ppm. These CO_2 levels are considered typical for the sulfur-bearing glasses with carbon impurities.

Thermal stability

Violet glass samples were heated in air. At approximately 900 °C the violet color started to diminish within an hour; this was accompanied by the formation of bubbles. The violet color was stable in air at 700 °C for at least 11 days. At elevated pressure, the violet color was stable to temperatures above 1500 °C. These experiments show that the violet color is associated with a volatile component that is stable at high temperatures.

Microprobe analyses: Sulfur peak positions

The location of the sulfur peak position changes by approximately 0.052 ° 2θ (0.10 mm on the PET crystal on the JEOL microprobe spectrometer used) when the immediate environment of the sulfur atom changes (Carroll and Rutherford 1988). This change corresponds to a change from sulfide (S^{2-}) to sulfate (S^{6+}). The shape and location of the sulfur peak was measured over the range 171.80 to 172.18 mm for samples and standards of sulfides and sulfates. The ratio of sulfide to sulfate in the sample was estimated by minimizing the difference between the peak observed for the sample and a peak calculated as a linear combination of the peaks for barite and sphalerite standards. This ratio was converted to a percentage of sulfide. The percentage of sulfide is based

TABLE 4. Examples of sulfur peak positions in different standards and samples

Sample	Total sulfur (ppm)	Peak position relative to barite (mm)	% Sulfide (est.)	Interpretation
ZnS		+0.109	100	
PbS		+0.101	95	
FeAsS		+0.094	89	
FeS_2		+0.088	82	The covalent bond makes pyrite different from the above sulfides
S, yellow		+0.088	~87	S-S bonds
S, orange		+0.079	~83	S-S bonds, larger spacing
$SrSO_4$		+0.005	−2	S-O bonds, "typical" sulfate.
$BaSO_4$		0.000	0	S-O bonds, "typical" sulfate.
0107	1589	−0.004	7	almost clear glass
0126, profile B, point 3	448	+0.001	7	0% of max. sulfur
0126, profile B, point 9	482	−0.011	1	0% of max. sulfur
0126, profile B, point 15	618	+0.002	3	29% of max. sulfur
0126, profile B, point 17	878	−0.009	1	73% of max. sulfur
0126, profile B, point 19	980	+0.004	2	97% of max. sulfur
0126, profile B, point 23	984	+0.012	5	100% of max. sulfur
0313, 30 μm into graphite	2339	+0.090	76	Sulfide, e.g., CS_2
0313, 90 μm from graphite (dark rim between violet glass and graphite)	3282	+0.01	7	Even close to the graphite sulfate dominates; sulfate is very stable.
0313, 1040 μm from graphite	1952	+0.010	4	Violet glass.
0613, very near Zr metal	1300	−0.004	9	
0613, very near Ti metal	1151	−0.002	13	
0626	1421	+0.002	10	
0628, Clear glass	944	+0.009	10	
1030, profile 6, point 23	1399	+0.003	12	99% of max. sulfur
1030, profile 6, point 33	1189	+0.011	20	83% of max. sulfur
1030, profile 6, point 38	694	+0.020	33	63% of max. sulfur
1030, profile 6, point 43	446	+0.037	41	38% of max. sulfur
1030, profile 6, point 47	339	+0.016	39	20% of max. sulfur
1030, profile 6, point 49	412	+0.099	80	14% of max. sulfur
1030, profile 6, point 53	202	+0.104	86	6% of max. sulfur

Note: Barite peak position 171.906 mm. For diffusion profiles the location within the profile is given as a percent of the sulfur in the doped half of the diffusion couple.

on the assumption that all sulfur is present as sulfide or as sulfate; if other species like S_2^- and S_3^- are present, this percentage becomes percent sulfide equivalents.

The results in Table 4 provide some representative examples of sulfur peak positions and calculated sulfide percentages in various glasses and standards. The results show that the peak position does not differ significantly between violet (e.g., sample 0313) and colorless (e.g., sample 0628) sulfate-bearing glasses. If the violet color is caused by S_2^- and S_3^- (as suggested by the spectroscopic analyses discussed below) this probably means that the concentration of S_2^- and S_3^- radical anions is relatively low and that sulfate is the dominant sulfur species. It is likely that the lack of change in sulfur peak position reflects a similarity in peak positions of S_2^-, S_3^-, and sulfate. Exactly what peak position these species have is difficult to evaluate because there are no pure standards. However, given that elemental sulfur has a peak position corresponding to 85% sulfide it is likely that S_2^- and S_3^- have peak positions that also fall close to the sulfide peak.

Table 4 also shows that sulfur diffused into graphite (sample 0313) has a peak position corresponding to a high sulfide content, indicating formation of carbon sulfides (most likely CS_2). Violet sulfur + carbon-bearing glass 90 μm from a graphite source (Experiment 0313, 4–7% sulfide) or a few tens of mircometers away from sheets of metallic Ti and Zr (Experiment 0613, 8–13% sulfide) show that even this close to reducing materials the sulfur is maintained as sulfate rather than sulfide. The implication is that the sulfate is very stable under the experimental conditions, even at very low values of f_{O_2}.

Visible and ultraviolet light absorption spectroscopy

Samples of albite glass, albite glass containing carbon, albite glass with sulfate (few violet spots), and albite glass with both carbon and sulfur (with the characteristic violet color) were investigated by both visible and UV spectroscopy. The albite glass shows a large absorbance in the UV range. The spectrum of the violet glasses exhibits two strong absorption peaks not found in any of the other samples, one at 570 nm and one at 400 nm. Combined with the Raman spectroscopy data discussed below, these absorption bands are attributed to S_3^- and S_2^-, respectively (Clark et al. 1983). S_4^- could potentially have been present in the samples; however, the characteristic absorption band of S_4^- was not observed.

Raman spectroscopy

Presented in Figure 2 are representative vibrational Raman spectra of the glasses. The results from all the Ra-

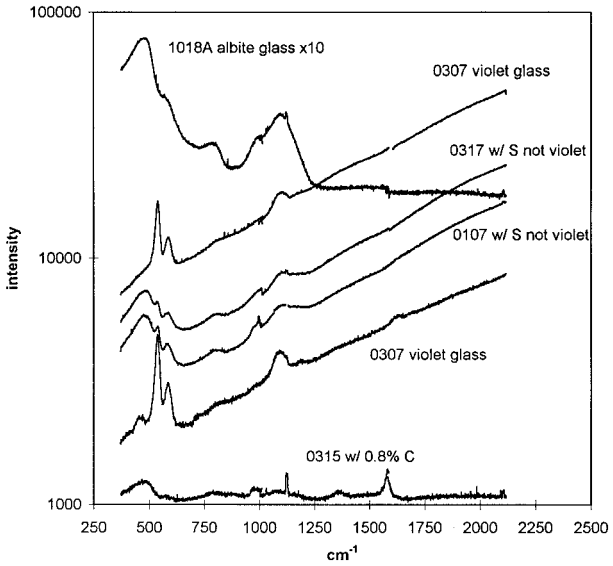

FIGURE 2. Raman spectra comparing albite glasses with and without sulfur and carbon. To improve the clarity of this figure the *y* axis is logarithmic and the pure albite glass signal has been multiplied by a factor 10.

man experiments are summarized in Table 5. Pure albite glass exhibits Raman shifts of 476, 588, 810, and 1096 cm^{-1}, which are associated with Si-O-Si and Al-O-Si stretching and bending vibrational modes. In addition to the albite glass peaks, the Raman spectra from violet-colored, sulfur-bearing glasses exhibit an enhanced background-scattering level and Raman shifts, which are assigned to fundamental and overtone vibrations of S_2^- and S_3^-. Using the work of Clark and Franks (1975) and Clark et al. (1983) as a basis for the assignment, the fundamental and the first two overtones for the S_2^- and S_3^- symmetric stretching modes are assigned as follows:

	S_2^-	S_3^-
Fundamental, ν	583–588 cm^{-1}	535–540 cm^{-1}
First overtone, 2ν	1184–1187 cm^{-1}	1094–1101 cm^{-1}
Second overtone, 3ν	1755 cm^{-1}	1625 cm^{-1}

The presence of the normally very weak overtone Raman scattering coupled with the fact that the excitation wavelength of 514.5 nm lies within the wings of both the 400 and 570 nm absorption bands of S_2^- and S_3^-, respectively, implies that scattering from S_2^- and S_3^- is the result of the resonance-enhanced Raman effect. Additional evidence

TABLE 5. Summary of selected Raman peaks and their interpretation

Peak (cm^{-1})	Depolarization ratio, ρ	Albite	Albite w/C	Albite w/CO_2	Albite w/CO_2 + NO_x	Albite w/CO_2 + H_2O	Albite w/S	Albite w/S + C	Albite w/S + C by spot	Interpretation
color		clear	black	black	clear	milky	clear	violet	violet	
215								—	x	
241	0.31							x		
264								x	x	
377–400		x	x	x	x		x			
476	0.00	X	X	X	X		X	(x)		Si-O-Si bending
481						x				
535–540	0.52							X		S_3^- (v)
585		x	x	x	x		x			
583–588	0.52							X		S_2^- (v)
702			x	x	x		x?			
793–810		X	x	x	x		x	x		Si-O-Si or Si-O-Al
980		x	x	x	x	x	x	(x)		$Si\text{-}O^-$
988						x				
1066						x				
1094		X	x	x	x	x	X			Si-O-Si
1094–1101								X	X	S_3^- (2v)
1122 (sharp)		x	X	x	x	x	(x)	x	x	
1184–1187								x	x	S_2^- (2v)
1313								x		
1348				x					x	CO_2
1355–1362			x							
1546									x	
1576									x	
1581–1585			X							
1599				x						
1625										S_3^- (3v)
1634			(x)					x		OH^-
1755									x	S_2^- (3v)
1937								x		
1944									x	
2106		x	x			—	x	—	—	
background		flat	flat	flat	flat	flat	weak slope	slope	slope	

X = very strong peak; X = strong peak; x = peak visible; (x) = occasionally visible; blank field = no peak. If the position was outside the range scanned it is marked with an "—". Peak identifications based on Fuxi 1992; Hibben 1939; Kubicki and Stolper 1995; Meites 1963.

for the resonance-enhanced Raman effect with 514.5 nm excitation comes from experiments using an excitation wavelength of 1064 nm. When a 1064 nm excitation source is used, none of the bands assigned to S_2^- and S_3^- were observed in the Raman spectra. Several other Raman shifts are only observed in spectra from the violet glasses (514.5 nm excitation). These are the 264, 718, 917, 1313, 1348, 1546, 1576, 1937, and 1944 cm^{-1} shifts that for the most part are weak peaks in the Raman spectra. Depolarization ratios were also obtained for the S_2^- and S_3^- symmetric stretching fundamental peaks. The depolarization ratio, ρ, is defined as the ratio of scattered light intensities with polarizations that are perpendicular and parallel to the plane polarized excitation light ($I_\perp/I_{//}$). For a perfectly symmetrical stretch, ρ will be zero and for a strongly asymmetric vibrational mode it will be nearly 0.75. The scattering from both of these fundamentals yields a depolarization ratio of 0.5. Such a depolarization ratio would not be inconsistent with one end of S_2^- and S_3^- being bound more strongly to the melt structure than the other end.

The sulfate group, SO_4^{2-}, is also present in the glasses as seen from the X-ray peak positions. However, because there is no resonance Raman effect for the sulfate at 514.5 nm excitation and the concentration is low, the characteristic Raman spectrum of sulfate is not observed in the spectra obtained from the glasses. S_4^- could also potentially have been present in the samples. Using the 1064 nm laser line for excitation, one might expect resonance-enhanced Raman scattering due to S_4^- because it possesses a strong electronic absorption band in the red wavelength region. However, none of the characteristic peaks of S_4^- were found (384, 439, 518, and 815 cm^{-1}; Clark and Cobbold 1978). CS_2 has two characteristic lines, 655 and 796 cm^{-1} (Hibben 1939); however, neither line was observed.

Electron spin resonance (ESR)

Electron spin resonance, ESR (or electron paramagnetic resonance, EPR) is a well-established technique for studying free radicals with a single unpaired electron. Exposing the sample to a strong magnetic field makes it possible to increase the energy separation between the two spin states of the unpaired electron. The sample absorbs electromagnetic energy at the frequency corresponding to the energy splitting between the two spin states. Sample 0426 (powdered violet glass) generated a good ESR spectrum showing that the sample actually does contain unpaired electrons. The spectrum shows evidence for the presence of two overlapping spectra implying two distinct radicals. The data are consistent with S-ions in a rhombic environment with a g tensor $g_1 = 2.037$, $g_2 = 2.020$, and $g_3 = 1.992$. There is, in addition, an overlapping weaker spectrum. The stronger spectrum compares well with the data of Lunsford and Johnson (1973) reported for S_3^-. However, to prove this result positively it would be necessary to prepare ^{34}S-doped samples, which was not done.

Sulfur compounds

Sulfate is stabilized over sulfide at values of f_{O_2} that are two orders of magnitude lower in an Na_2O-$3SiO_2$ melt than in an andesite-dacite melt (Carroll and Rutherford 1988; Baker and Rutherford 1996). This large increase in stability primarily reflects the effect of having different elements available (or not available) for forming sulfide bonds: Na and Si have a far smaller tendency to form sulfides than metals like Fe and Mn, which are present in natural andesites and dacites. Although a natural magma will form sulfides at values of f_{O_2} close to the Ni-NiO buffer (Baker and Rutherford 1996), albite melt may not. Instead reactions of the following type can take place:

$$3C + 2MSO_4 \leftrightarrow 3CO_2 + (2MO)^+ + S_2^- \quad (1)$$

$$9C + 6MSO_4 \leftrightarrow 9CO_2 + (6MO)^+ + S_3^- \quad (2)$$

where M is Na_2, $Al_{3/4}$, or $Si_{1/4}$. These reactions are in agreement with the observation that S_2^- and S_3^- are formed and the amount of CO_2 is higher in the violet than in the non-violet sulfur-bearing glasses, although only by a few tens of parts per millions. However, as CO_2 diffuses relatively fast through the melt, some of the CO_2 generated will be lost. Although the radical anions S_2^- and S_3^- are not that common, they are found in ultramarine blue and S_3^- is found in small quantities in lazurite (lapis lazuli) (Clark et al. 1983).

In samples containing residual graphite as well as CO_2, the f_{O_2} is probably at 1400 °C more than 3 log units below Ni-NiO (Huebner 1971). At this f_{O_2} Nagashima and Katsura (1973) reported that less than 20% of the sulfur in an Na_2O-$3SiO_2$ melt is sulfate whereas the remainder is sulfide. However, the albite melt studied here has sulfate as the dominant sulfur species at this f_{O_2}. The difference can be a result of differences in the level of trace elements (like iron), or it could arise because in albite melt every Na is paired with an Al, which does not happen in the Na_2O-$3SiO_2$ melt.

Concentration of S_2^- and S_3^-

Figure 3 shows a diffusion profile with the combined S_2^- and S_3^- radical anion (relative) concentration plotted in addition to total sulfur concentration. The S_2^- and S_3^- peak intensities were measured relative to a Si-O-Si Raman peak at 476 cm^{-1} and used to estimate the relative concentration of these species. Because the ratio between the two species, S_2^- and S_3^-, is constant along a diffusion profile at a given temperature, Figure 3 shows only a combined $S_2^- + S_3^-$ concentration plotted on an arbitrary scale. It is seen that the variations in $S_2^- + S_3^-$ concentration mimics the variations in ''sulfide'' concentration along the profile and it cannot be ruled out that the ''sulfide'' measured using the X-ray peak shift is actually S_2^- and S_3^-. Given that the $S_2^- + S_3^-$ concentration cannot exceed the total sulfur measured with the microprobe, and that the highest $S_2^- + S_3^-$ concentrations are measured at a point in the diffusion profile where the total sulfur is 400 ppm, the concentration of $S_2^- + S_3^-$ must at all times

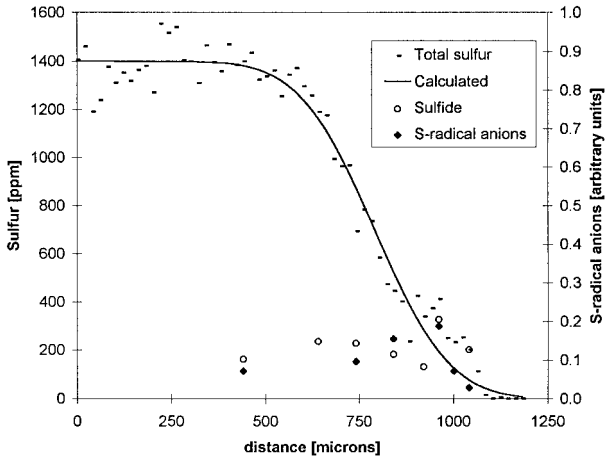

FIGURE 3. Example of sulfur diffusion profile from sample 1030. The solid black line shows the calculated profile used in finding the D-value. At selected points the ''sulfide'' concentration has been calculated from the X-ray peak position assuming that the observed peak is a combination of the peaks for sulfate (barite) and sulfide (sphalerite). In reality a substantial amount of this calculated ''sulfide'' is likely to be S_2^- and S_3^-. The relative variations in S_2^- and S_3^- are shown on an arbitrary scale (right) because there have been no absolute concentration measurements of these species.

be below that level. In a sample with 1400 ppm total sulfur, the data in Figure 3 show that the ''normal'' violet glass has less than 200 ppm of $S_2^- + S_3^-$. Even at this concentration level the sample has a strong violet color. Some samples without the violet color have X-ray peaks indicating that part of the sulfur is present as sulfide, e.g., 0626 containing nitrite shows 9% ''sulfide'' whereas clear areas of 0107 show 7% ''sulfide''. This means that not all of the apparent ''sulfide'' is caused by S_2^- and S_3^-.

Sulfur attachment to melt structure

The depolarization ratios for the main S_2^- and S_3^- peaks are both measured around 0.50–0.52 in the albite glass. Because S_2^- is a diatomic molecule the fundamental Raman band should be polarized (depolarization ratio 0) for the free ion. The bent S_3^- anion has been found to have a depolarization ratio of 0.23 in a liquid solution (Clark and Cobbold 1978). Using a simplistic model in which the increase in depolarization ratio is attributed to the bonding of one end of S_2^- or S_3^- with the silicate framework, we can estimate the degree to which S_2^- or S_3^- is bound in the glasses. Because these results are obtained on glasses, not directly on the melt, there is no direct proof that these hypothesized attachments reflect the structure of the melt at higher temperature. However, it is very likely that an anion like S_2^- or S_3^-, would form some sort of bond to structural elements in the melt.

If [S] is the concentration of a free (mobile) sulfur-bearing species (e.g., S_2^-, S_3^-, SO^{2-}_4, or S^{2-}) and [N] is the concentration of suitable attachment sites in the network, the equilibrium of the reaction S + N ↔ SN determines how many S units are in average free to move at any given time and how many units are tied to the melt structure. This equilibrium has an equilibrium constant K = [SN]/([S][N]). In this simplistic model, the depolarization ratio can be used (at least qualitatively) to estimate this ratio: if [SN] = 0 the depolarization ratio would be close to zero (no asymmetry), whereas if the more molecules are bound in one end (higher [SN]) then the depolarization ratio is higher.

Spectra have been obtained from samples with various S_2^- and S_3^- concentrations and they have all shown the same depolarization ratios, indicating that the ratio [SN]/[S] is constant based on the above assumptions. This implies that the [N] term is dominant. Therefore the number of available sites where the sulfur species can bind is very large compared to the amount of sulfur present. The depolarization ratio was also found to be the same near the low sulfur concentration end of the diffusion profile in sample 1030. If the bonding to the network were slow, this part of the diffusion profile should be dominated by ''free'' sulfur species. However, the data imply the opposite.

The bond-making/bond-breaking reaction must take place rapidly compared to the rate of diffusion. A rapid ''reaction'' rate means that significant changes may have time to occur during quenching and that detailed in-situ (high temperature) spectroscopic studies will be required to achieve a full understanding of these aspects of melt structures and diffusion. This type of work is important from the point of view of understanding how much of the sulfur is actively diffusing and how fast the ''truly free'' sulfur diffuses.

The presence of carbon (resulting in the formation of S_2^- and S_3^-) and/or the presence of Fe possibly promoting more sulfide in the melt (sulfide solubility increases with Fe in the melt, Haughton et al. 1974 and Mathez 1976), helps change the state of sulfur so the overall diffusivity increases. This illustrates how the entire chemical environment, not just parameters like the f_{O_2} level, determines the ''physical behavior'' of elements like sulfur.

EXPERIMENTAL RESULTS: SULFUR DIFFUSION

Activation energy of diffusion

Figure 3 shows an example of a sulfur diffusion profile and Table 2 summarizes the results. Experiments at 1400 °C and 1 GPa were performed with different run times and with different sulfur concentrations in each end of the diffusion couples: approximately 0–400, 400–1200, and 0–1200 ppm. The results show that the diffusion coefficients do not change significantly with either time or concentration within the ranges investigated. They also show that the results are reproducible. Experiments were performed at 1300, 1400, and 1500 °C (Fig. 4 and Table 2). The results can be fitted to an Arrhenius-type relation given by the equation $D = D_0 \exp(-Q/RT)$, from which the activation energy, Q (= 458.1 ± 50.8 kJ/mol), and pre-exponential factor, D_0 (= 14.7 ± 39.1 m^2/s), have

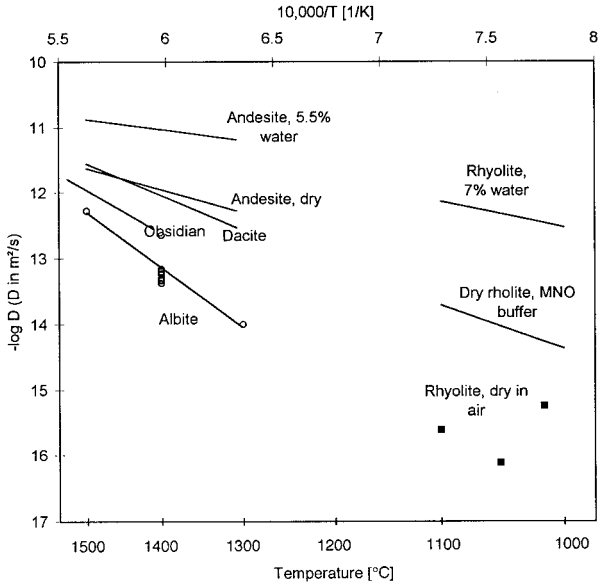

FIGURE 4. Arrhenius type plot showing the relationship between temperature and diffusion coefficients for various magma compositions. Albite data are from this study. Rhyolite (dry in air, dry at MNO and 7% water) is from Baker and Rutherord (1996). The remaining data are from Watson et al. (1993).

been calculated, with $r^2 = 0.988$. The calculations are based on average values from Table 2. At 1642 °C this activation energy and pre-exponential factor give a diffusion coefficient close to the value calculated from the data of Baker and Rutherford (1996) for sulfur diffusion in a dry rhyolitic melt at 13–200 kPa and buffered at MNO (short for $MnO\text{-}Mn_3O_4$). However, their equation was not calibrated above 1100 °C, so the significance of the similarity is uncertain. At lower temperatures their D values become larger than the values found here. This difference is due probably to the different melt composition and to the possible difference in sulfur species involved in the diffusion. Interestingly, the new sulfur diffusitivities for albite resemble earlier values for dry obsidian obtained under reducing conditions (Watson 1994) and for dry rhyolite obtained under very oxidizing (in air) conditions (Baker and Rutherford 1996).

Species diffusing

Five different species could be participating in the diffusion observed in the experiments: S_2^-, S_3^-, S^{2-}, SO_4^{2-}, or S^{6+}. The fastest-diffusing form will have a major influence on the overall diffusion rate. There are three ways by which we can gain insight into what species are actually responsible for the mass transport: variations in sulfide/sulfate ratios along the diffusion profile; variation in bulk diffusion with different degrees of violet coloration; and variations in the Raman intensity of the S_2^- and S_3^- peaks along the diffusion profile. Figure 3 shows a diffusion profile where total sulfur, sulfide, and relative $S_2^- + S_3^-$ are shown as a function of distance. The sulfide is calculated from the sulfate/sulfide ratio based on the X-ray peak shift and the total sulfur concentration. As explained previously, part of this ''sulfide'' may actually be S_2^- and S_3^- if their X-ray peak falls close to the sulfide peak position. The amount of sulfate is total sulfur minus the ''sulfide'' (not shown on Figure 3).

It is remarkable that in sample 1030 (Fig. 3), the $S_2^- + S_3^-$ and ''sulfide'' goes up in the diffusion zone and does not drop until the very end of the diffusion profile. This can be interpreted to mean that S_2^- and S_3^- diffuse faster than the sulfate, which, in view of size and charge arguments, is not unreasonable.

In some other profiles (samples 0124 and 0126) the sulfide/sulfate ratio stays more constant throughout the diffusion profile and apparently these samples have experienced a faster equilibration between S_2^-/S_3^- and sulfate; variations in the f_{o_2} may cause this. These profiles also show diffusion coefficients lower than sample 1030, consistent with the conclusion that sulfate diffuses more slowly than S_2^- and S_3^-.

Samples 0702, 0707, and 0718 (Table 2) contained an oxidant ($NaNO_3$) and were less strongly violet then the other samples. These samples show larger diffusion coefficients, however, perhaps because the oxidant forms dissolved water by combining with hydrogen in the setup.

Baker and Rutherford (1996) concluded that under all but the most oxidizing (in air) conditions, the principal species diffusing is the sulfide ion (S^{2-}). As seen in Figure 4, their results indicate that in very oxidized samples the diffusion rate is roughly 2 orders of magnitude slower, showing that the SO_4^{2-} is very slowly diffusing. The albite melt investigated here contains very little (if any) sulfide, even at very low f_{o_2}, and S_2^- and S_3^- must diffuse significantly faster than the SO_4^{2-} group. The results found in this study are thus compatible with the results of Baker and Rutherford (1996): the diffusion is dominated by sulfide, S_2^-, and S_3^-, whereas SO_4^{2-} diffuses very slowly. In albite, where sulfate is the dominating species, the overall diffusion is very slow—slower, in fact, than any of the other melts shown in Figure 4.

The $3S_2 \leftrightarrow 2S_3$ reaction

The $S_2^-/(S_2^- \cdot S_3^-)$ Raman peak size ratio varies by 5% across the profile shown for sample 1030 in Figure 3, and that there are no systematic trends in the variations. Any apparent variations most likely reflect analytical uncertainties. Because the larger S_3^- is likely to move more slowly than the smaller but similarly charged S_2^-, this result shows that the equilibration between the two species is fast relative to the diffusion process. A possible reaction between the two species is:

$$(xMO)^+ + 3S_2^- \leftrightarrow (xMO) + 2S_3^- \quad (3)$$

Effective diffusion radius

There could be two different reasons why the albite shows lower D values than any of the other melts: (1) the diffusion is controlled by different sulfur species and/or

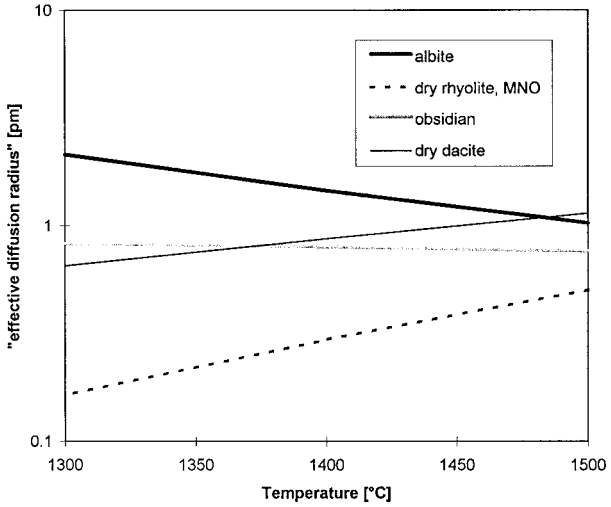

FIGURE 5. Effective diffusion radius shown as a function of temperature. This radius is not the actual physical radius of the diffusing species. The effective diffusion radius is used as a tool for comparing differences in diffusivity after having eliminated the effect of differences in melt viscosity. The melt viscosities used in the calculations were based on Bottinga and Weill (1972) assuming that there is no change with pressure and that all melts are dry. All experiments, except for the rhyolite, were done at 1 GPa, whereas the rhyolite was investigated at lower pressure. If the pressure effect is taken into account, the 1 GPa values will move to larger radii, more than the rhyolite values will, making the difference between the rhyolite and the rest larger (based on results from Scarfe et al. 1979). If the small amounts of water in the albite melt is taken into account, the albite line will move to larger radii values corresponding to a slower viscosity adjusted diffusion, separating it from the rest of the melts. All viscosity calculations were based on coefficients for the 0.75–0.81 mole fraction SiO_2 range.

(2) the albite melt is significantly more polymerized, and has a much higher viscosity, than the other melts. Although the Stokes-Einstein equation does not provide a reliable tool for calculating diffusion coefficients in melts of this type (e.g., Liang et al. 1996), it is reasonable to assume that there still will be an inverse proportionality between diffusion coefficients and melt viscosity. The Stokes-Einstein equation has been rearranged to provide an ''effective diffusion radius,'' $r = kT/6\pi\eta D$, where k is the Boltzmann constant, T is the temperature in K, η is the viscosity, and D the diffusion coefficient. The radius calculated here does not correspond to the radius of the actual species diffusing and is exclusively used as a tool for comparing differences in diffusivities over and above the effect of viscosity: The larger the effective diffusion radius the slower the effective diffusivity. Figure 5 shows a plot where the effective diffusion radius is plotted as a function of temperature for some of the melts shown in Figure 4. If the relationship between viscosity and temperature is the same as the relationship between the diffusion coefficient and viscosity, all lines should be horizontal in this diagram. The lines for sulfur in dry rhyolite and obsidian are, within error, horizontal. The slope of the line for S_2^-/S_3^--bearing albite may result from the uncertainty on the temperature dependence of the D value: The value at 1400 °C is well determined whereas only a couple of results exist for other temperatures. It could also reflect a change in the relative amounts of S_2^- and S_3^- over temperature, suggesting that at higher temperatures there is more of the smaller (and faster diffusing) S_2^-. Given the uncertainty on the determinations of diffusion coefficients and melt viscosities the ''viscosity-corrected diffusivity'' of sulfur in albite melt is only slightly slower than it is in obsidian and dry dacite. The dry rhyolite (Baker and Rutherford 1996), despite a composition almost identical to the obsidian, has a somewhat higher diffusivity. This difference could be caused by differences in sulfur speciation and experimental techniques. If the S_2^- and S_3^- are the rate-controlling species for diffusion in the albite melt, and if sulfide is primarily controlling the diffusion in the obsidian and the dacite, then it appears that the sulfide has a similar or slightly higher rate of diffusion. This conclusion does not, however, take into account how large a fraction of the sulfur is present as very slow-diffusing sulfate.

Based on the results presented in Figure 5, the effective diffusion radius is 8.4×10^{-13} m for sulfide-controlled diffusion, 1.5×10^{-12} m for S_2^-/S_3^--dominated diffusion, and much larger still for sulfate-controlled diffusion. This effective diffusion radius takes into account the effect of size as well as bonding to the melt structure. The effective diffusion radius of S_2^-/S_3^- is a factor 1.8 higher than for sulfide. The real radius, not effective diffusion radius, of an S atom (likely to equal the smallest radius of an $S\text{-}S^-$ or $S\text{-}S\text{-}S^-$ molecule) is 1.6 times larger than the radius of an S^{2-} ion. Taking all uncertainties into account there is no real difference between the values of 1.6 and 1.8. This result indicates that size is a large part of the explanation for the difference in diffusivity. Raman spectroscopy has shown that the S_2^-/S_3^- molecules with a valence of -1 do form bonds to the glass structure (and presumably as well to the melt structure); these bonds are, however, likely to be weaker than the bonds formed to the sulfide ion with a valence of -2. On the other hand, the S_2^-/S_3^- radical anions are longer than the round sulfide ion and thus are hindered in their diffusion.

CONCLUSIONS

Sulfur can occur in magmas as sulfate, sulfide, S_2^- or S_3^-. The melt composition, in particular the presence or absence of chalcophile elements, and the f_{O_2} determine which sulfur species will be present. It was found that in the presence of carbon under reducing conditions, the radical anions S_2^- or S_2^- form in low concentrations. The sulfate diffuses significantly more slowly than the other species (sulfide, S_2^-, or S_3^-), which means that at high f_{O_2} and in the absence of chalcophile elements the diffusion of sulfur slows down significantly. To compare diffusivities in melts of different compositions an ''effective diffusion radius'' was calculated. Although the Stokes-

Einstein equation is known to be invalid for this type of melt, it is assumed that the inverse relationship between melt viscosity and diffusivity nevertheless holds. In this way the calculated radius does not correspond to the actual radius of the species diffusing but it serves as a gauge of viscosity-independent diffusion. It is suggested that these ''effective diffusion radii'' can be used to estimate the diffusion coefficients in any melt as long as the melt viscosity can be estimated accurately at the temperature in concern.

Acknowledgments

This work was supported by NSF grant no. EAR-9406914 to E.B. Watson. Daniel Moore and Daniele Cherniak are thanked for their contributions to this work. Leslie Baker and Simon Poulson are thanked for their valuable comments. The following are thanked for their assistance with analytical work: Tom Apple (RPI-spectroscopy techniques) , Peter Codella (GE-Raman), Steve Crichton (RPI-FTIR), Todd Przybycien and Samir Sane (RPI-Raman), Joseph Warden (RPI-ESR spectrum and interpretation), David Wark (RPI-microprobe).

References cited

Baker, L.L. and Rutherford, M.J. (1996) Sulfur diffusion in rhyolite melts. Contributions to Mineralogy and Petrology, 123, 335–344.

Bradbury, J.W. (1983) Pyrrhotite solubility in hydrous albite melts, 136 p. Ph.D. thesis, Pennsylvania State University, University Park, Pennsylvania.

Bottinga, Y. and Weill, D.F. (1972) The viscosity of magmatic silicate liquids: a model for calculation. American Journal of Science, 272, 438–475.

Carroll, M. and Rutherford, M.J. (1988) Sulfur speciation in hydrous experimental glasses of varying oxidation state: results from measured wavelength shifts of sulfur X-rays. American Mineralogist, 73, 845–849.

Clark, R.J.H. and Cobbold, D.G. (1978) Characterization of Sulfur Radical Anions in solutions of Alkali Polysulfides in Dimethylformamide and Hexamethylphosphoramide and in the Solid State in Ultramarine Blue, Green, and Red. Inorganic Chemistry, 17, 3169–3174.

Clark, R.J.H., Dines, T.J., and Kurmoo, M. (1983) On the nature of the sulfur chromophores in ultramarine blue, green, violet, and pink and of the selenium chromophore in ultramarine selenium: characterization of radical anions by electronic and resonance Raman spectroscopy and the determination of their excited-state geometries. Inorganic Chemistry, 22, 2766–2772.

Clark, R.J.H. and Franks, M.L. (1975) The Resonance Raman Spectrum of Ultramarine Blue. Chemical Physics Letters, 34, 69–72.

Cotton, F.A., Harmon, J.B., and Hedges, R.M. (1976) Calculation of the ground state electronic structures and electronic spectra of di- and trisulfide radical anions by the scattered wave-SCF-X alpha method. Journal of the American Chemical Socciety, 98, 1417–24.

Fincham, C.J.B. and Richardson, F.D. (1954) The behaviour of sulphur in silicate and aluminate melts. Proceedings of the Royal Society of London, Series A, Mathematical and Physical Series, 223, 40–61.

Fine, G. and Stolper, E. (1985) The speciation of carbon dioxide in sodium aluminosilicate glasses. Contributions to Mineralogy and Petrology, 91, 105–121.

Fuxi, G. (1992) Optical and Spectroscopic Properties of Glass, 283 p. Springer-Verlag, Berlin.

Gerlach, T.M. and Nordlie, B.E. (1975a) The C-O-H-S gaseous system, part I: composition limits and trends in basaltic cases. American Journal of Science, 275, 353–376.

———(1975b) The C-O-H-S gaseous system, part II: temperature, atomic composition, and molecular equilibria in volcanic gases. American Journal of Science, 275, 377–394.

———(1975c) The C-O-H-S gaseous system, part III: magmatic gases compatible with oxides and sulfides in basaltic magmas, American Journal of Science, 275, 395–410.

Haughton, D.R., Roeder, P.L., and Skinner, B.J. (1974) Solubility of sulfur in mafic magmas, Economic Geology, 69, 451–467.

Hibben, J.H. (1939) The Raman Effect and its Chemical Applications, 544 p. Reinhold Publishing Corporation, New York.

Huebner, J.S. (1971) Buffering techniques for hydrostatic systems at elevated pressures. In G.C. Ulmer, Ed., Research techniques for high pressure and high temperature, p. 123–178. Springer-Verlag, New York.

Kress, V. (1997) Magma mixing as a source for Pinatubo sulphur. Nature, 389, 591–593.

Kubicki, J.D. and Stolper, E.M. (1995) Structural roles of CO_2 and $[CO_3]_2$- in fully polymerized sodium aluminosilicate melts and glasses. Geochimica et Cosmochimica Acta, 59, 683–698.

Liang, Y., Richter, F.M., Davis, A.M., and Watson, E.B. (1996) Diffusion in silicate melts: I. Self diffusion in CaO-Al_2O_3-SiO_2 at 1500°C and 1 GPa. Geochimica et Cosmochimica Acta, 60, 4353–4367.

Lunsford, J.H. and Johnson, D.P. (1973) Electron paramagnetic resonance study of S_3^- formed on magnesium oxide. Journal of Chemical Physics, 58, 2079–2083.

Mathez, E.A. (1976) Sulfur solubility and magmatic sulfides in submarine basalt glass. Journal of Geophysical Research, 81, 4269–4276.

Meites, L. (1963) Handbook of Analytical Chemistry, McGraw Hill Book Co., Inc., New York.

Mysen, B.O. and Dick, H.J.B. (1977). Solubility of volatiles in silicate melts under the pressure and temperature conditions of partial melting in the upper mantle; Magma genesis 1977; proceedings of the American Geophysical Union Chapman conference on partial melting in the Earth's upper mantle. Bulletin-Oregon, Department of Geology and Mineral Industries, 96, 1–14.

Mysen, B.O. and Popp, R.K. (1980) Solubility of sulfur in $CaMgSi_2O_6$ and $NaAlSi_3O_8$ melts at high pressure and temperature with controlled f_{O_2} and f_{S_2}. American Journal of Science 280, 78–92.

Nagashima, S. and Katsura, T. (1973) The solubility of sulfur in Na_2O-SiO_2 melts under various oxygen partial pressures at 1100, 1250 and 1300°C. Bulletin of the Chemical Society of Japan, 46, 3099–3103.

Poulson, S.R. and Ohmoto, H. (1990) An evaluation of the solubility of sulfide sulfur in silicate melts from experimental data and natural samples. Chemical Geology, 85, 57–75.

Ricke, W. (1960) Ein beitrag zur geochemie des schwefels. Geochimica et Cosmochimica Acta, 21, 35–80.

Scarfe, C.M., Mysen, B.O., and Virgo, D. (1979) Changes in Viscosity and Density of Melts of Sodium Disilicate, Sodium Metasilicate, and Diopside Composition with Pressure. Annual Report of the Director, Geophysical Laboratory, Carnegie Institution 1978–1979, 1978 Yearbook.

Silver, L. and Stolper, E. (1989) Water in Albitic Glass. Journal of Petrology, 30, 667–709.

Watson, E.B. (1994) Diffusion in volatile bearing magmas. In Mineralogical Society of America Reviews in Mineralogy, 30, 371–411.

Watson, E.B. Wark, D.A., and Delano, J.W. (1993) Initial report on sulfur diffusion in magmas. EOS, 74, 620p.

Manuscript received January 6, 1998
Manuscript accepted July 18, 1998
Paper handled by David London